CrystEngComm

Accepted Manuscript

ROYAL SOCIETY OF CHEMISTRY

www.rsc.org/crystengcomm

Journal Name

RSCPublishing

ARTICLE

Unconventional upright layer orientation and considerable enhancement of proton-electron conductivity in Dion-Jacobson perovskite thin films

Cite this: DOI: 10.1039/x0xx00000x

Received 00th January 2012,
Accepted 00th January 2012

DOI: 10.1039/x0xx00000x

www.rsc.org/

Tomohiko Nakajima,*[a] Kiyoshi Kobayashi,[b] Kentaro Shinoda[a] and Tetsuo Tsuchiya[a]

Excimer-laser-assisted metal organic deposition is a straightforward process for growing uniaxially oriented Dion-Jacobson perovskite thin films. We have confirmed that on amorphous glass substrates, Dion-Jacobson phases normally crystallize and become oriented with layer-stacking ordering, for example, in $RbLa_2Ti_2NbO_{10}$ and $RbLaNb_2O_7$ thin films under KrF laser irradiation. Here, we observed a unique orientation in $RbCa_2Nb_3O_{10}$ thin films, where almost perfect upright layered structures were realized on amorphous glass substrates. The precursor $RbCa_2Nb_3O_{10}$ thin film crystallized with uniaxial (100)-orientation under KrF laser irradiation with a fluence above 100 mJ/cm^2 and with a preference for (100)- and (001)-orientation below 100 mJ/cm^2. The obtained (100)-oriented $RbCa_2Nb_3O_{10}$ thin films showed extremely high proton-electron conductivity of 4.9×10^{-2} S/cm at 400 °C.

Introduction

The conducting properties of oxide thin films are strongly dependent on crystal quality. In particular, crystal orientation control is among the most important issues in preparing oxide thin film materials with excellent properties, where the crystal orientation is generally controlled by using a substrate with a specially designed surface structure. Single-crystal oxide substrates are preferred in research on oxide thin films because they enable precise control of the surface structure and yield high orientation quality in crystal growth.[1–5] However, the use of single-crystal oxide substrates is not feasible for industrial applications due to their high cost and small size. Therefore, excimer-laser-assisted metal organic deposition (ELAMOD) was recently developed as a method for growing oxide thin films with high orientation quality without using single-crystal substrates. It is a straightforward process for growing perovskite thin films with almost perfect uniaxial orientation on amorphous substrates.[6–8] ELAMOD is based on chemical solution deposition (CSD) and can be used to fabricate oxide thin films at low temperature for commonly used substrates such as Si and borosilicate glass, which cannot withstand high temperatures (greater than 400 °C) in air. In ELAMOD, oxide films crystallize under excimer laser irradiation instead of under heating in a high-temperature furnace, as in the MOD process.[6,9,10] Details of the crystal growth mechanism in this process are described elsewhere.[6,11,12] We have so far successfully prepared Dion-Jacobson perovskite $RbLaNb_2O_7$ thin films with almost perfect uniaxial orientation on amorphous glass substrates by ELAMOD.[7,8] Dion-Jacobson perovskites have a general formula $AA'_{n-1}B_nO_{3n+1}$ (A = alkaline metal ion or proton, A' = alkaline earth or rare earth ion, B = transition metal ion, n = layer number) and show a typical two-dimensional crystal structure, where the A cations and layered perovskite slabs are stacked alternately (Fig. 1).[13–17] We examined the uniaxial growth mechanism in terms of spatial heating based on the gradient temperature distribution near the film surface under photothermal heating in ELAMOD. We found that under gradient heating by excimer laser irradiation, the first nucleation occurred preferentially at the film surface with layered structural ordering to reduce the crystal surface energy. Then, the film was epitaxially grown downward from the first layer-oriented crystal nuclei, leading to almost perfect uniaxial orientation of the $RbLaNb_2O_7$ thin film.[7]

In this study, we observed unique upright layer orientation instead of layer stacking in Dion-Jacobson phases grown under excimer laser irradiation. Upright layer orientation is extremely rare, and to our knowledge, this is the first case where such a structure was obtained without being induced by the underlying substrate lattice. The interlayer sites of perovskite slabs in the Dion-Jacobson phase have numerous attractive properties such

as high ion conductivity,[18–21] photocatalytic reactivity,[22–24] and strong potential for use in the fabrication of new nanoarchitectures by intercalation for fascinating applications such as superconductors and low-dimensional magnetic materials.[25–28] The upright layer orientation provides numerous gates to such sites at the surface, and therefore crystals grown in this way are expected to show new properties. Here, we report the details of the conditions for oriented growth and the orientation dependence of conductivity of the Dion-Jacobson perovskites $RbCa_2Nb_3O_{10}$ (RCNO, n = 3), $RbLa_2Ti_2NbO_{10}$ (RLTNO, n = 3), and RLNO (n = 2) (Fig. 1).

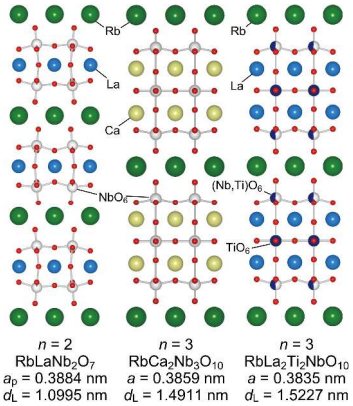

Fig.1 Schematic illustrations of crystal structure of $RbLaNb_2O_7$, $RbCa_2Nb_3O_{10}$, and $RbLa_2Ti_2NbO_{10}$.

Experimental Section

Thin film fabrication

RCNO thin films were fabricated by ELAMOD. The starting solutions for the RCNO films were prepared by mixing carboxylate solutions of the constituent metals Rb (SYM-RB03, Symetrix), Ca (SYM-CA05, Symetrix), and Nb (niobium 2-ethylhexanoate, Azmax). RLTNO thin films were fabricated by ELAMOD. The starting solutions for the RLTNO films were prepared by mixing carboxylate solutions of the constituent metals Rb (SYM-RB03, Symetrix), La (SYM-LA01, Symetrix), and Nb (niobium 2-ethylhexanoate, Gelest). These solutions were spin-coated onto silica glass substrates at 4000 rpm for 10 s. The coated films were preheated at 400 °C in air for 10 min to transform the precursor amorphous oxide films by decomposing the coated organic components. The procedure from spin coating to preheating was repeated three times to increase the film thickness. The precursor amorphous films were irradiated with a KrF laser (Compex110, Lambda Physik) at a fluence of 25–115 mJ/cm^2 and a pulse duration of 26 ns for 7500 pulses at 400 °C in air. Oriented RLNO thin films were also prepared on silica glass substrates by ELAMOD, where the preparation conditions were the same as previously reported.[7] To compare the effect of film orientation on conductivity, we also prepared unoriented RCNO, RLTNO, and RLNO films by conventional MOD at 950 °C in air for 60 min.

Sample characterization

The structural and orientation properties of the obtained films were studied with an X-ray diffractometer (SmartLab, Rigaku) using $2\theta/\omega$ and $2\theta\chi/\phi$ scans. We obtained 2θ-β maps (β: direction along Debye rings) using a two-dimensional pixel area detector (PILATUS 100K, Dectris)[29] and a collimator with diameter of 200 μm. The distance between the detector and the sample was fixed at 120 mm. The degree of orientation was evaluated in terms of the Lotgering factor F, which is calculated using the following equation:[30]

$$F(hkl) = \frac{P - P_0}{1 - P_0}$$

Here, $P_0 = \Sigma(I_0(hkl))/\Sigma(I_0(HKL))$ and $P = \Sigma(I(hkl))/\Sigma(I(HKL))$. I_0 is the intensity of a diffraction peak in an XRD pattern in the Inorganic Crystal Structure Database, and I is that determined experimentally. The crystal growth process and crystallinity of the thin films were observed by cross-sectional transmission electron microscopy (XTEM) using a microscope (H-9000NAR, Hitachi) operated at 300 kV. The samples for XTEM observations were prepared by the focused ion beam method.
The electrical conductivity of in-plane geometry with a 200 μm probe distance was measured with an LCR meter (6440A, Wayne Kerr) in dry and wet H_2 atmosphere. The frequency for the impedance measurements was varied from 20 Hz to 3 MHz. The H^+/D^+ isotope effect on the electrical conductivity was also measured in H_2O/Ar and D_2O/Ar. In each case, the atmosphere was humidified by bubbling the carrier gas through water (H_2O or D_2O) at ambient temperature.

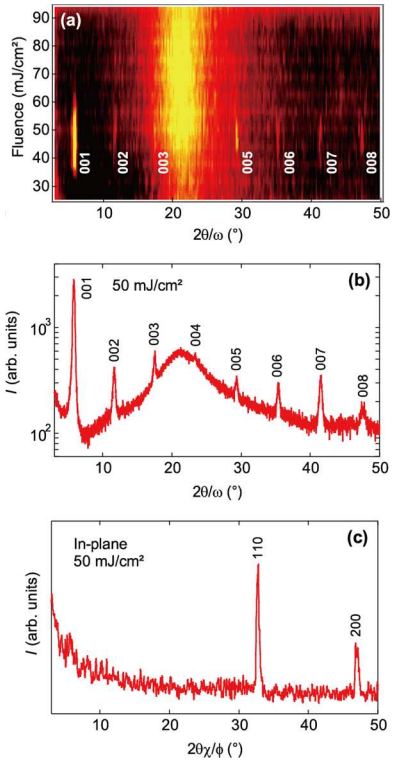

Fig. 2 (a) XRD intensity map as a function of laser fluence for RLTNO thin films on a silica substrate. (b) Out-of-plane $2\theta/\omega$ and (c) in-plane $2\theta\chi/\phi$ scans at 50 mJ/cm^2.

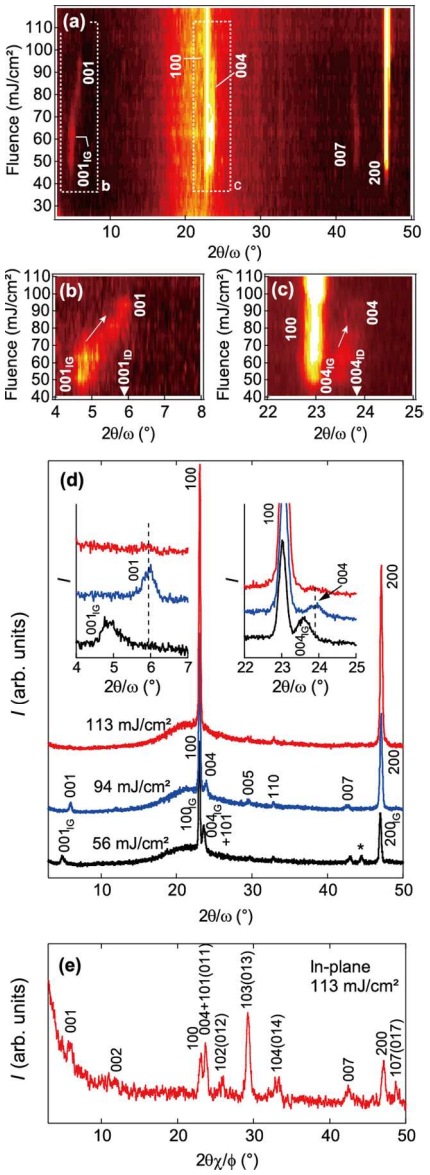

Fig. 3 (a–c) XRD intensity map as a function of laser fluence for RCNO thin films on silica substrates. (d) Out-of-plane $2\theta/\omega$ scan at 56, 94, and 113 mJ/cm^2. (c) In-plane $2\theta\chi/\phi$ scan at 113 mJ/cm^2. IG indicates the intergrowth phase, and ID indicates the ideal peak position for bulk RCNO.

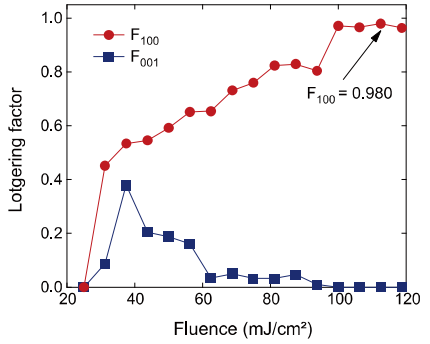

Fig. 4 Fluence dependence of Lotgering factors F_{100} and F_{001} for (100)- and (001)-orientations of the RCNO films, respectively.

Results and Discussion

Crystal growth and orientation of Dion-Jacobson perovskites with n=3

Figure 2a shows the $2\theta/\omega$ of XRD pattern as a function of KrF laser fluence for the RLTNO film prepared by ELAMOD on a silica glass substrate at 400 °C. In the range of 35–65 mJ/cm^2, RLTNO films crystallized and only 00*l* diffraction peaks appeared, and the peak intensity reached a maximum at a fluence around 45–50 mJ/cm^2. The $2\theta/\omega$ and $2\theta\chi/\phi$ scans of XRD patterns at 50 mJ/cm^2 are shown in Figs. 2b and 2c. All out-of-plane peaks were assigned to the 00*l* reflection, and only orthogonal peaks corresponding to 110 and 200 for the 00*l* reflection were observed in the in-plane diffraction pattern. The Lotgering factor for (001) (F_{001}) was calculated to be 1.0, indicating perfect (001)-orientation (layer stacking). The crystal orientation and growth behavior for RLTNO films are extremely similar to those for previously reported RLNO thin films.[7] Furthermore, we confirmed that many other Dion-Jacobson phases, such as $CsLaNb_2O_7$ and $KLaNb_2O_7$, show a growth mode similar to that of RLTNO and RLNO, which are likely realized according to the aforementioned proposed mechanism.[7]

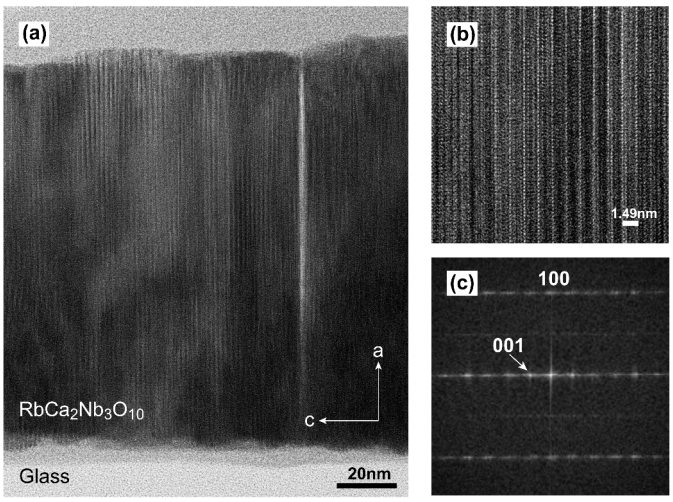

Fig. 5 (a) [010]-zone XTEM image for an RCNO thin film on a silica glass substrate after irradiation with a KrF laser at a fluence of 113 mJ/cm^2 for 7500 pulses. (b) High-resolution image of the RCNO film. (c) Calculated electron diffraction pattern of the oriented film at the same position as in (b).

However, RCNO showed a completely different orientation. Figure 3a–c shows the $2\theta/\omega$ XRD pattern as a function of KrF laser fluence for the RCNO film prepared by ELAMOD on a silica glass substrate at 400 °C. At low fluence of 40–65 mJ/cm^2, the diffraction peaks were assigned to *h*00 and 00*l* reflections, however, the lattice parameter *c* was 22% longer than the ideal value for the RCNO phase.[16] This could be due to intergrowth of the layered structure of RCNO. The elongated *c*-axis returned to the ideal value as fluence increased to 65–100

mJ/cm^2, although (100)- and (001)-orientations were still observed. Above 100 mJ/cm^2, all 00l peaks disappeared and strongly preferred (100)-orientation was eventually realized (Fig. 3a–c). The out-of-plane and in-plane X-ray diffraction patterns at 113 mJ/cm^2 showed h00 and 0kl peaks, respectively, indicating the preferred (100)-orientation (Fig. 3d,e).

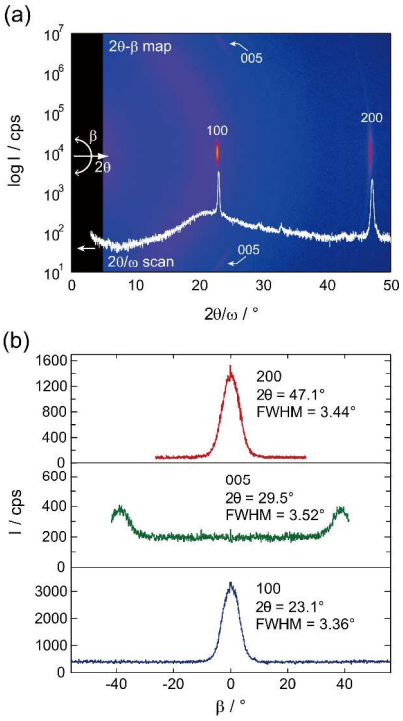

Fig. 6 XRD 2θ/ω–β map and 2θ/ω scan for the RCNO film after KrF laser irradiation at 113 mJ/cm^2, and β-scan profiles of 200, 005, and 100 reflections for the RCNO film.

The Lotgering factors F_{100} and F_{001} for the (100)- and (001)-orientations were calculated as shown in Fig. 4. F_{100} gradually increased and F_{001} gradually decreased with increasing laser fluence in two steps. The first step corresponded to adjusting the fluence to a value at which the elongated c-axis became ideal for RCNO, and in the second step the fluence was increased to a value at which the (001)-orientation disappeared (F_{001} = 0). The maximum F_{100} = 0.98 was observed at 113 mJ/cm^2, which indicates almost perfect (100)-orientation.

The XTEM image of the RCNO thin film prepared at 113 mJ/cm^2 (Fig. 5) provides strong evidence for the preferential (100)-orientation. This high-resolution image shows clear periodicity (d = 1.49 nm) corresponding to a layered structure of RCNO which is perpendicular to the substrate normal. The orientation quality of the RCNO film was examined from the 2θ-β map (Fig. 6). The Bragg reflections corresponding to h00 indices appeared as spot-like reflections at β = 0°, and the weak reflections for the 005 index were also observed from the same domain of (100)-oriented film at around β = 40°. The β scan profile for 100, 005, and 200 reflections collected from the obtained 2θ-β map showed an obvious peak, and the full width at half-maximum (FWHM) of h00 reflections was around 3.4°. This value is small for amorphous glass substrates and indicates high crystal orientation quality. On the basis of this structural analysis, we confirmed that the fabricated RCNO film at strong laser fluence exhibited high uniaxial orientation quality in the (100) plane. The perfect upright layer ordering structure observed in this study is exceptionally rare, and to our knowledge this is the first case where such a structure was obtained without being induced by the substrate lattice.

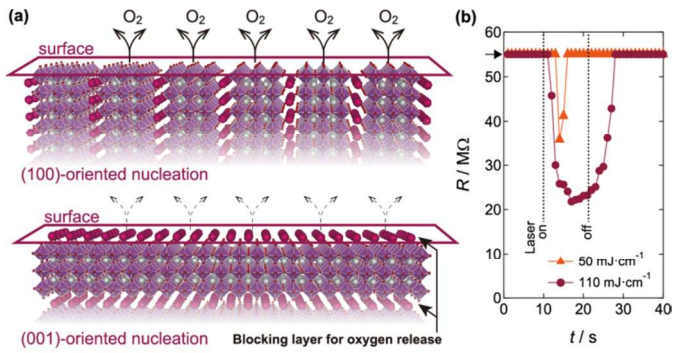

Fig. 7 (a) Schematic illustrations of partial oxygen deficiency in the (100)- and (001)-oriented RCNO films for the first nucleation at the surface under KrF laser irradiation. (b) Resistance for the RCNO films during KrF laser irradiation at a fluence of 50 and 110 mJ/cm^2 for 50 Hz at 400 °C as a function of time. The arrow represents the measurement limit at 55 MΩ.

The possible driving force to form the upright layer orientation could be related to partial oxygen deficiency at first nucleation near the surface under the photothermal gradient heating due to strong laser irradiation in addition to the preferred crystal facet growth. Firstly, the RCNO crystal seems to have similar facet growth property with the RLNO which has the layered structure as well as the RCNO (Fig. 1). The calculated facet area of the RLNO crystal indicated that the (100)-orientation (upright layer type) was second preferential growth direction, followed by the (001)-orientation (layer stacking type).[8] Here, we have so far observed partial oxygen deficiency at film surface of oxide thin films under excimer laser irradiation with a strong laser fluenece above 70–80 mJ/cm^2 in some oxides such as TiO_2 and $LaNiO_3$.[31,32] Especially, a partial upright layer type ordering has been observed in $LaNiO_3$.[32] The oxygen ions in $LaNiO_3$ can be defected, and the oxygen deficient $LaNiO_3$ is known to be $LaNiO_2$ as a stable phase. Under KrF laser irradiation, oxygen deficient layer was aligned orthogonally to the substrate normal ((100)-orientation). This indicates that the [100]-direction of perovskite slabs in the RCNO would be effective for the oxygen release compared to the [001]-paths through Rb ion layers (Fig. 7a). Although there is no stable oxygen deficient and defect aligned phase in the RCNO, on the basis of these points, it could be enough as a driving force for first (100)-oriented nucleation at the top surface if there is instantaneous oxygen deficiency of the perovskite slabs by strong laser irradiation in the RCNO.

Figure 7b shows the electrical resistance for the precursor RCNO thin films with the KrF laser irradiation at 50 and 110 mJ/cm^2 at 50 Hz for 11 s during the measurements. A slight response was observed in the resistance at 50 mJ/cm^2 during the

laser irradiation. At 110 mJ/cm^2, the resistance was clearly reduced during the laser irradiation, and it was recovered to insulator completely after a few seconds from the laser switched off. This detectable conductivity was caused by partial reduction of Nb ions to tetravalent due to the oxygen deficiency, and supports our proposed mechanism for the upright layer orientation. The anisotropic pathways for oxygen release could be a very interesting controlling factor for orientation growth of oxide thin films under photothermal gradient heating by the laser irradiation.

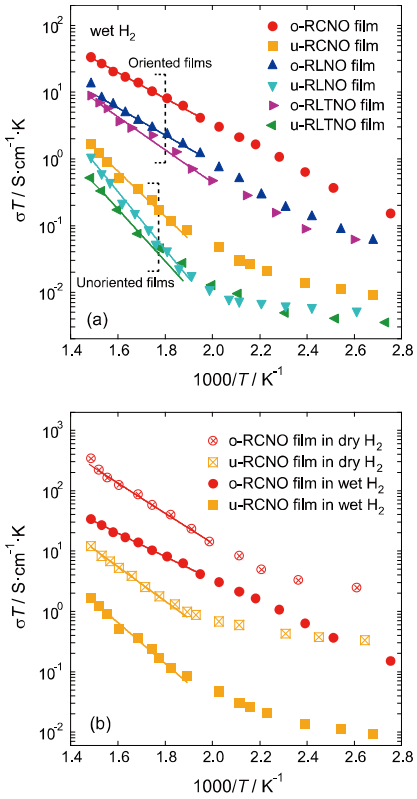

Fig. 8 (a) Arrhenius plots of electrical conductivity for o- and u-RCNO, RLTNO, and RLNO thin films in wet H_2 atmosphere. (b) Arrhenius plots of electrical conductivity for o- and u-RCNO thin films in wet and dry H_2. Solid lines represent fits.

Effect of film orientation on the conductivity of Dion-Jacobson perovskites

A promising application of the upright layer orientation of Dion-Jacobson phases would be proton conduction due to the open structure of inter-layer sites. High proton conductivity of Dion-Jacobson phases derived from proton substitution at inter-layer alkaline metal sites has already been reported.[18–21] Here, we studied the proton conductivity of the prepared samples. Figure 8a shows Arrhenius plots for the electrical conductivity (σ) of oriented (o-) and unoriented (u-) RCNO, RLTNO, and RLNO thin films in wet H_2 atmosphere. Table 1 lists σ at 400 °C and the calculated activation energy (E_a) in the range of 250–400 °C. The observed σ and calculated E_a for the oriented samples are clearly much higher and lower than those of the unoriented samples, respectively. Also, the linearity of Arrhenius plots for the oriented films is considerably higher than that for the unoriented ones until the low-temperature region at around 100 °C. Among the oriented samples, RCNO with upright layer ordering showed the highest conductivity of 4.9×10^{-2} S/cm at 400 °C. Additionally, E_a was lowest at 0.33 eV for o-RCNO. Relatively unobstructed carrier hopping in o-RCNO is realized by arrayed the transport pathways and large number of active sites at the surface in contact with the atmosphere.

Table 1. Electrical conductivity of o- and u-RCNO, RLTNO, and RLNO thin films.

Material	σ / S·cm^{-1}	E_a / eV	Atmosphere
o-RCNO	4.9×10^{-2}	0.33	Wet H_2
o-RCNO	5.0×10^{-1}	0.44	Dry H_2
u-RCNO	2.4×10^{-3}	0.62	Wet H_2
u-RCNO	1.8×10^{-2}	0.51	Dry H_2
o-RLTNO	1.9×10^{-2}	0.35	Wet H_2
u-RLTNO	1.6×10^{-3}	0.81	Wet H_2
o-RLNO	1.3×10^{-2}	0.44	Wet H_2
u-RLNO	7.7×10^{-4}	0.72	Wet H_2

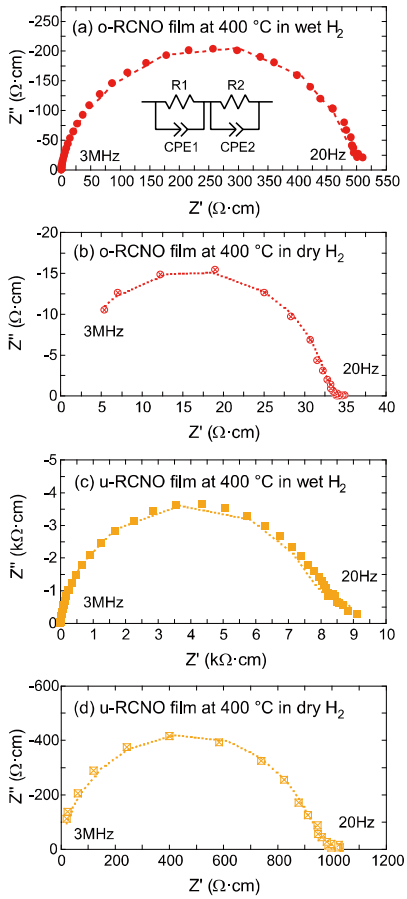

Fig. 9 Impedance spectra for o- and u-RCNO thin films in wet and dry H_2 at 400 °C in the range of 20 Hz to 3 MHz. Dotted lines are fits obtained using an (*RC*)-(*RC*) equivalent circuit, as shown in the inset of (a).

Table 2. Parameters obtained from fits to impedance spectra of o- and u-RCNO, RLTNO, and RLNO thin films.

Material	R_1 / Ω·cm	C_1 / nF·cm^{-2}	P_1	R_2 / Ω·cm	C_2 / nF·cm^{-2}	P_2	Atmosphere
o-RCNO	428	375	0.935	65.5	566	0.939	Wet H_2
o-RCNO	32.7	8.43	0.954	1.52	2590	0.88	Dry H_2
u-RCNO	7850	6.68	0.938	1400	3190	0.818	Wet H_2
u-RCNO	922	1.89	0.937	86.7	6630	0.729	Dry H_2

Figure 8b shows the conductivity of o- and u-RCNO films in wet and dry H_2 atmospheres. In both cases, the conductivity in dry H_2 was around 10-fold that in wet atmosphere. In dry H_2, electron conduction is enhanced by producing oxygen vacancies, followed by a reduction of Nb ions from pentavalent to tetravalent via a reaction of hydrogen with lattice oxygen. Figure 9 shows the impedance spectra of o- and u-RCNO films in wet and dry H_2 atmospheres at 400 °C. Curve fitting was carried out by an (*RC*)-(*RC*) type equivalent circuit using a constant phase element (CPE), where the impedance of CPE (Z_{CPE}) is calculated from the equation $Z_{CPE} = 1/C(j\omega)^p$ (C is a capacitance when $p = 1$, j is the imaginary unit, ω is the frequency, and p is a dimensionless coefficient related to the distribution of relaxation time). Lower resistivity in dry H_2 was observed in the impedance spectra in both cases. The spectra consisted of the main semicircle and a small tail at low frequencies. The fitted parameters of these data are listed in Table 2. Although the parameters for the second *RC* circuit do not seem to have sufficient accuracy due to insufficient analysis at the low frequency region below 20 Hz (measurement limit), the capacitance C_1 corresponding to the main semicircle, which is related to the overall geometric capacitance, showed a clear trend toward lower values as a result of changing the atmosphere from wet to dry H_2. This means that the enhancement in electron conduction in RCNO thin films is likely due to the reduction of Nb ions.

Additionally, we examined the isotope effect on conductivity of the o-RCNO film in humidified Ar atmospheres using vaporized H_2O and D_2O. Figure 10 shows σ of the o-RCNO film at room temperature in H_2O/Ar and D_2O/Ar, where σ clearly decreased and increased by 9% as a result of changing the atmosphere from H_2O/Ar to D_2O/Ar and from D_2O/Ar to H_2O/Ar, respectively. This provides clear evidence of proton conduction in this system. The σ variation is theoretically expected to be $\sigma(H_2O)/\sigma(D_2O) = \sqrt{2}$ (*ca.* 21%) in pure proton conductors,[33] and therefore we concluded that the obtained o-RCNO film is a proton-electron mixed conductor.

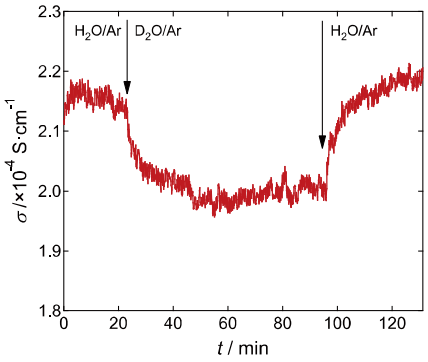

Fig. 10 Isotope effect on electrical conductivity of the o-RCNO film in humidified Ar atmosphere containing vaporized H_2O or D_2O at room temperature.

Thus, we demonstrated that o-RCNO has a strong potential to serve as an ion conductor owing to the aligned transport paths in upright layer oriented RCNO films while still showing electron conductivity ($\sigma = 4.9 \times 10^{-2}$ S/cm at 400 °C). In fact, film orientation clearly had a strong effect on conductivity: at 270 °C, σ of o-RCNO in dry H_2 was two orders of magnitude higher than that of reported bulk pellets.[18] A proton conductivity greater than 10^{-2} S/cm at 200–500 °C (this temperature range is important for intermediate-temperature fuel cells) has been rarely observed. It appears as a gap in the phase diagram for proton conductors that are strong candidates for use as electrodes in solid oxide fuel cells as reported by Norby.[34] Therefore, the structure with upright layer ordering is expected to fill this gap in Norby's diagram by further enhancing proton conduction.

Conclusion

ELAMOD is a straightforward process for growing uniaxially oriented Dion-Jacobson perovskite thin films. On amorphous glass substrates, Dion-Jacobson phases normally crystallize and become oriented with layer stacking, such as in the RLTNO and RLNO thin films under KrF laser irradiation. However, we observed a unique orientation in RCNO thin films, where an almost perfect upright layered structure was realized on amorphous glass substrates. The precursor RCNO thin film crystallized with strong (100)-orientation under KrF laser irradiation with fluence above 100 mJ/cm^2 and with mixed preference for (100)- and (001)-orientation below 100 mJ/cm^2. The obtained (100)-oriented RCNO film showed exceptionally high conductivity of 4.9×10^{-2} S/cm at 400 °C and was evaluated as a proton-electron mixed conductor based on analysis impedance and the isotope effect.

Acknowledgements

This work was partly supported by Grant-in-Aid for Young Scientists (B) No. 25820338 from the Japan Society for the Promotion of Science.

Notes and references

[a] Advanced Manufacturing Research Institute, National Institute of Advanced Industrial Science and Technology, Tsukuba Central 5, 1-1-1 Higashi, Tsukuba, Ibaraki 305-8565, Japan.
[b] National Institute for Materials Science, 1-2-1 Sengen, Tsukuba, Ibaraki 305-0047, Japan.

1 A. Brinkman, M. Huijben, M. Vanzalk, J. Huijben, U. Zeitler, J. C. Maan, W. G. van der Wiel, G. Rijnders, D. H. A. Blank and H. Hilgenkamp, *Nature*, 2007, **6**, 493.
2 I. Vrejoiu, M. Alexe, D. Hesse and U. Gösele, *Adv. Funct. Mater.*, 2008, **18**, 1.
3 S. J. May, P. J. Ryan, J. L. Robertson, J.-W. Kim, T. S. Santos, E. Karapetrova, J. L. Zarestky, X. Zhai, S. G. E. te Velthuis, J. N. Eckstein, S. D. Bader and A. Bhattacharya, *Nat. Mater.*, 2009, **8**, 892.
4 Y. Wakabayashi, D. Bizen, H. Nakao, Y. Murakami, M. Nakamura, Y. Ogimoto, K. Miyano and H. Sawa, *Phys. Rev. Lett.*, 2006, **96**, 017202.
5 S. A. Chambers, *Adv. Mater.*, 2009, **21**, 1.
6 T. Nakajima, K. Shinoda and T. Tsuchiya, *Chem. Soc. Rev.*, 2014, DOI: 10.1039/c3cs60222b.
7 T. Nakajima, T. Tsuchiya and T. Kumagai, *Cryst. Growth Des.*, 2010, **10**, 4861.
8 T. Nakajima, T. Tsuchiya and T. Kumagai, *CrystEngComm*, 2011, **13**, 158.
9 T. Tsuchiya, K. Daoudi, T. Manabe, I. Yamaguchi and T. Kumagai, *Appl. Surf. Sci.*, 2007, **253**, 6504.
10 T. Tsuchiya, I. Yamaguchi, T. Manabe, T. Kumagai and S. Mizuta, *Mater. Sci. Semicond. Process*, 2003, **5**, 207.
11 T. Nakajima, T. Tsuchiya, M. Ichihara, H. Nagai and T. Kumagai, *Chem. Mater.*, 2008, **20**, 7344.
12 T. Nakajima, T. Tsuchiya, M. Ichihara, H. Nagai and T. Kumagai, *Appl. Phys. Express*, 2009, **2**, 023001.
13 M. Dion, M. Ganne and M. Tournoux, *Mater. Res. Bull.*, 1981, **16**, 1429.
14 J. Gopalakrishnan, V. Bhat and B. Raveau, *Mater. Res. Bull.*, 1987, **22**, 413.
15 A. R. Armstrong and P. A. Anderson, *Inorg. Chem.*, 1994, **33**, 4366.
16 M. J. Geselbracht, R. I. Walton, E. S. Cowell, F. Millange and D. O'Hare, *Chem. Mater.,* 2002, **14**, 4343.
17 M. J. Geselbracht, H. K. White, J. M. Blaine, M. J. Diaz, J. L. Hubbs, N. Adelstein and J. A. Kurzman, *Mater. Res. Bull.,* 2011, **46**, 398.
18 V. Thangadurai and W. Weppner, *J. Mater. Chem.,* 2001, **11**, 636.
19 M. Sakthivel and W. Weppner, *J. Phys. D: Appl. Phys.,* 2007, **40**, 7210.
20 Y. Kobayashi, J. A. Schottenfeld, D. D. Macdonald and T. E. Mallouk, *J. Phys. Chem. C,* 2007, **111**, 3185.
21 J. A. Schottenfeld, Y. Kobayashi, J. Wang, D. D. Macdonald and T. E. Mallouk, *Chem. Mater.,* 2008, **20**, 213.
22 M. Machida, T. Mitsuyama, K. Ikeue, S. Matsushima and M. Arai, *J. Phys. Chem. B,* 2005, **109**, 7801.
23 H. G. Kim, O. S. Becker, J. S. Jang, S. M. Ji, P. H. Borse and J. S. Lee, *J. Solid State Chem.,* 2006, **179**, 1214.
24 K. Maeda, M. Eguchi, W. J. Youngblood and T. E. Mallouk, *Chem. Mater.,* 2009, **21**, 3611.
25 K. G. Sanjaya Ranmohotti, E. Josepha, J. Choi, J. Zhang and J. B. Wiley, *Adv. Mater.,* 2011, **23**, 442.
26 M. Kato, A. Inoue, I. Nagai, M. Kakihana, A. W. Sleight and Y. Koike, *Physica C,* 2003, **388-389**, 445.
27 Y. Takeda, T. Momma, T. Osaka, K. Kuroda and Y. Sugahara, *J. Mater. Chem.,* 2008, **18,** 3581.
28 C. Tassel, J. Kang, C. Lee, O. Hernandez, Y. Qiu, W. Paulus, E. Collet, B. Lake, T. Guidi, M.-H. Whangbo, C. Ritter, H. Kageyama and S.-H. Lee, *Phys. Rev. Lett.,* 2010, **105**, 167205.
29 P. Kraft, A. Bergamaschi, Ch. Broennimann, R. Dinapoli, E. F. Eikenberry, B. Henrich, I. Johnson, A. Mozzanica, C. M. Schlepütz, P. R. Willmott and B. Schmitt, *J. Synchrotron Radiat.,* 2009, **16**, 368.
30 F. K. Lotgering, *J. Inorg. Nucl. Chem.,* 1959, **9**, 113.
31 T. Nakajima, T. Tsuchiya and T. Kumagai, *J. Solid State Chem.*, 2009, **182**, 2560.
32 T. Nakajima, T. Tsuchiya and T. Kumagai, *Appl. Phys. A*, 2011, **104**, 981.
33 N. Kurita, N. Fukatsu, K. Ito and T. Ohashi, *J. Electrochem. Soc.,* 1995, **142**, 1552.
34 T. Norby, *Solid State Ionics,* 1999, **125**, 1.

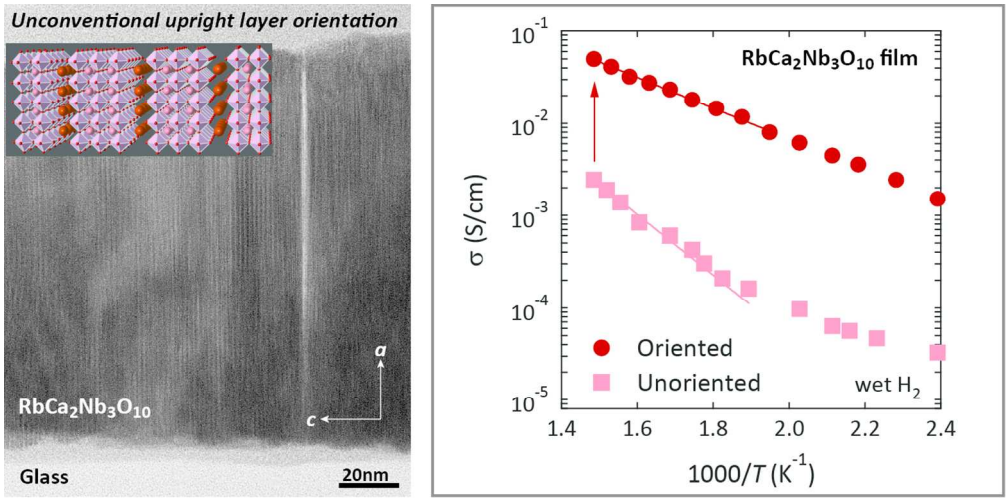

124x61mm (300 x 300 DPI)